applied sciences

MDPI

Communication

Magnetic Vortex Phase Diagram for a Non-Optimized $CaKFe_4As_4$ Superconductor Presenting a Wide Vortex Liquid Region and an Ultra-High Upper Critical Field

Armando Galluzzi [1,2,*], Antonio Leo [1,2], Andrea Masi [3], Francesca Varsano [4], Angela Nigro [1,2], Gaia Grimaldi [2] and Massimiliano Polichetti [1,2,*]

[1] Department of Physics "E.R. Caianiello", University of Salerno, Via Giovanni Paolo II, 132, 84084 Fisciano, SA, Italy
[2] CNR-SPIN Salerno, Via Giovanni Paolo II, 132, 84084 Fisciano, SA, Italy
[3] ENEA, Via Enrico Fermi, 45, 00044 Frascati, RM, Italy
[4] ENEA, Via Anguillarese, 301, 00123 Roma, Italy
* Correspondence: agalluzzi@unisa.it (A.G.); mpolichetti@unisa.it (M.P.)

Featured Application: This work concerns the study of the vortex phase diagram in $CaKFe_4As_4$, whose knowledge can be helpful for the understanding of the applicative ranges in field and temperature of these materials with not-optimized fabrication characteristics, as usually is found in superconducting wires and cables for power applications.

Abstract: To draw a complete vortex phase diagram for a $CaKFe_4As_4$ polycrystalline iron-based superconductor, different kinds of magnetic measurements have been performed focusing on the critical parameters of the sample. Firstly, magnetic moment versus field measurements m(H) were performed at low fields in order to evaluate the lower critical field H_{c1}. After that, by performing relaxation measurements m(t), a field crossover H_{cross} was detected in the framework of a strong pinning regime. The irreversibility field H_{irr} as a function of the temperature curve was then drawn by plotting the critical current densities J_c versus the field for temperatures near T_c. J_c(H) has demonstrated a second magnetization peak effect phenomenon, and the second peak field H_{sp} has been identified and plotted as a function of temperature, providing information about an elastic to plastic transition in the vortex lattice. Finally, the upper critical field H_{c2} as a function of the temperature has been obtained. H_{c1}, H_{cross}, H_{sp}, H_{irr}, H_{c2} have been fitted and used for drawing the complete vortex phase diagram of the sample. It can be helpful for the understanding of the applicative ranges in the field and temperature of the materials with not-optimized fabrication characteristics, as usually is found in superconducting wires and cables for power applications.

Keywords: iron-based superconductors; 1144 IBS family; pinning properties; irreversibility field; upper critical field; magnetism and superconductivity; power applications

Citation: Galluzzi, A.; Leo, A.; Masi, A.; Varsano, F.; Nigro, A.; Grimaldi, G.; Polichetti, M. Magnetic Vortex Phase Diagram for a Non-Optimized $CaKFe_4As_4$ Superconductor Presenting a Wide Vortex Liquid Region and an Ultra-High Upper Critical Field. *Appl. Sci.* **2023**, *13*, 884. https://doi.org/10.3390/app13020884

Academic Editor: Melvin M. Vopson

Received: 14 November 2022
Revised: 2 January 2023
Accepted: 6 January 2023
Published: 9 January 2023

1. Introduction

The iron based superconductors (IBS) found out in 2008 [1] are probably the most intriguing material to investigate since the high-T_c superconductors (HTS) discovery by Bednorz and Muller in 1986 [2]. In fact, although the HTS critical temperature T_c is well above the liquid nitrogen temperature in many cases, materials such as YBCO or BSCCO have been not exploited completely for their use in power applications of superconductivity due to some problems: high values of anisotropy [3,4], superconductor-insulator-superconductor (SIS) grain boundary junction [5,6]etc. On the other hand, although the IBS have a lower T_c than HTS, they show lower values of anisotropy [7,8] and superconductor-normal-superconductor (SNS) grain boundary junction [9,10] together with high values of J_c and H_{c2} [11,12]. Among all the IBS families, the recently discovered 1144 family has

attracted the attention of researchers due to its analogy in the crystal structure with the well-known 122 IBS family [13]. In the 1144 family, the $CaKFe_4As_4$ presents interesting peculiarities such as relatively high $T_c \approx 35$ K [14,15], large upper critical field [16,17], and very high J_c at high fields as well [17,18]. Moreover, in very recent years, $CaKFe_4As_4$ wires and tapes have been successfully fabricated by the powder-in-tube method [19,20] opening perspectives in terms of using this material for practical purposes. It is worth underlining that Refs. [19,20] have not performed a thorough magnetic analysis of the material nor the construction of a complete vortex phase diagram as instead shown in this work. The CaKFe4As4 can form during the fabrication process also spurious phases such as $CaFe_2As_2$ and KFe_2As_2 [14] and a large number of impurities. So, it is clear that the superconducting properties and critical parameters can be drastically enhanced if these phases and the grain boundaries formation are reduced by improving the fabrication process. In this framework, one of the most common problems in applications of superconducting materials on a large scale is the difficulty of not being able to optimize their superconducting characteristics in the entire volume of the application. In fact, the characteristics of such materials can differ particularly in the case of using well-optimized samples with perfect crystalline structure compared to when considering volumes of material much larger than a single crystal. In this context, the study of non-optimized samples becomes very useful to understand the field and temperature behavior of their superconducting critical parameters. In general, the first and third harmonic of the AC magnetic susceptibility is a valid approach to studying the vortex dynamics [21,22] but it often requires difficult analysis processes. In this context, it is worth underlining that an in-depth study of the temperature dependence of the modulus of the first and third harmonic of the AC magnetic susceptibility gives very accurate information about the vortex melting line [23,24]. The results are usually influenced by the values of the amplitude and frequency of the AC magnetic field together with the possibility to use a superimposed DC field. So, it reveals a very useful investigation when it is necessary to individuate the vortex melting line of the superconductor with well-fixed AC and DC field parameters. Alternatively, DC magnetization can be used. Its response as a function of the temperature, the magnetic field, and the time gives information about the critical parameters of the sample useful to draw a complete vortex phase diagram. In the present study, we report the superconducting properties of a non-optimized $CaKFe_4As_4$ superconductor by using DC magnetization measurements in magnetic fields up to 9 Tesla and temperatures in the range 5–35 K. In particular, the attention has been focused on drawing the vortex phase diagram of the sample. At this aim, different critical parameters such as H_{c1}, H_{irr}, etc. have been obtained. The results showed that the sample is perspective in terms of energy/high-power applications due to its very large H_{c2} values and the strong pinning behavior. Nevertheless, the observed very wide vortex liquid region makes us understand that the efficiency of the pinning is low. Then, the sample must be optimized by improving, for instance, the fabrication process.

2. Materials and Methods

A disk-shaped pellet having a diameter equal to 3 mm and a thickness equal to 0.65 mm has been analyzed by means of DC magnetic measurements. The sample has been obtained by using a mechanochemically assisted synthesis route [25]. The fabrication details are reported in Ref. [15]. The sample has been characterized by measuring the magnetic moment as a function of the temperature m(T), the magnetic field m(H), and the time m(t). The measurements have been performed in perpendicular field configuration (field applied perpendicular to the disk surface) by using a QD-PPMS doted of a vibrating sample magnetometer. The residual entrapped field in the PPMS superconducting magnet [26] has been decreased below 1×10^{-4} T by oscillating the field around zero [27]. For the m(T) measurements, the sample was cooled down to 2.5 K without a magnetic field. After that, the field was turned on and the data was acquired by increasing the temperature (Zero Field Cooling) up to 300 K. For the m(H) measurements, after cooling the sample at the target temperature, the field has been increased to +9 T, decreased to −9 T, and

finally increased again to +9 T. For the m(t) measurements, firstly the target temperature has been reached in zero fields. Then, a field equal to 8 T has been set and then decreased to the measurement field. After waiting for about 100 s for avoiding a metastable magnetic states [28], the data have been acquired for 10,800 s. Table 1 summarizes the measurement parameter values used in this work.

Table 1. Measurement parameters values.

Measurement	Minimum Value	Maximum Value	Rate
m(T)	2.5 K	300 K	0.5 K/min
m(H)	−9 T	+9 T	0.01 T/s
m(t)	100 s	10,800 s	1 datapoint/s

3. Results and Discussion

To draw the complete sample vortex phase diagram, the lower critical field H_{c1} has been the first studied critical parameter. In particular, the first magnetization was measured versus the field at several temperatures. In Figure 1, the m(H) curves have been reported up to 0.1 T at 5 K, 10 K, 15 K, 20 K, and 25 K. It is visible the initial linear behavior of the magnetic moment due to the Meissner state and the reduction of the superconducting signal due to the temperature increase.

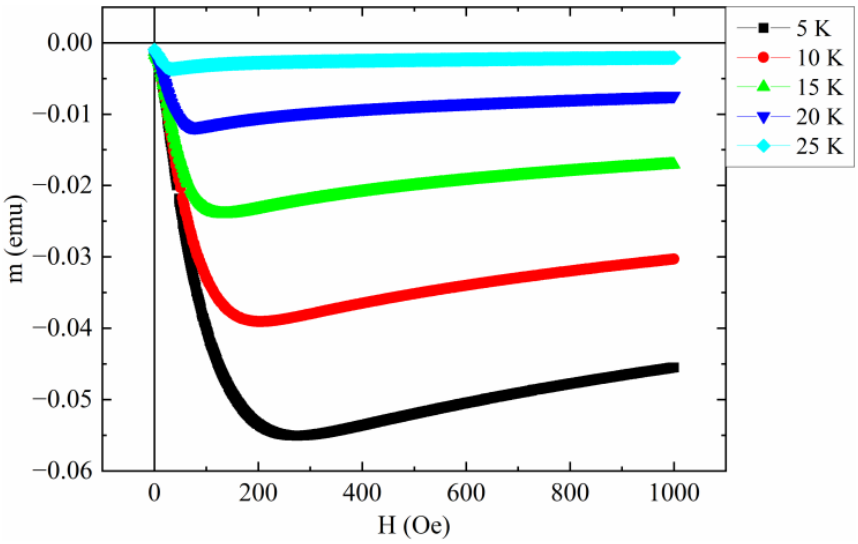

Figure 1. Field dependence of the magnetic moment at different temperatures in the range of low magnetic fields.

In the main panel of Figure 2, H_{c1} has been determined for T = 10 K. The dashed red line and the red arrow individuate the linear behavior due to the Meissner state and the H_{c1} value, respectively. Considering all the temperatures, the $H_{c1}(T)$ behavior has been obtained and fitted with the power law [29]:

$$H_{c1}(T) = H_{c1}(0)(1 - T/T^*)^n \quad (1)$$

where $H_{c1}(0)$ is the value of Hc1 at T = 0 K and T^* indicates when the phenomenon is undetectable. The $H_{c1}(T)$ curve together with its fit is reported in the inset of Figure 2. From the fit procedure, $H_{c1}(0) \approx 120$ Oe, $T^* \approx 27.7$ K, $n \approx 0.67$ have been obtained. The study of the $H_{c1}(T)$ line is interesting since below it the sample is in the Meissner state while above it the vortices start to enter the sample causing dissipation processes. From our previous work [15], we already know that a strong pinning regime characterizes our sample. Now, we want to determine how the vortex interact with each other by means of magnetic relaxation measurements. At this aim, m(t) measurements have been made at

several temperatures and fields. Figure 3 shows relaxation measurements at 2.5 K between 0.1 T and 1 T.

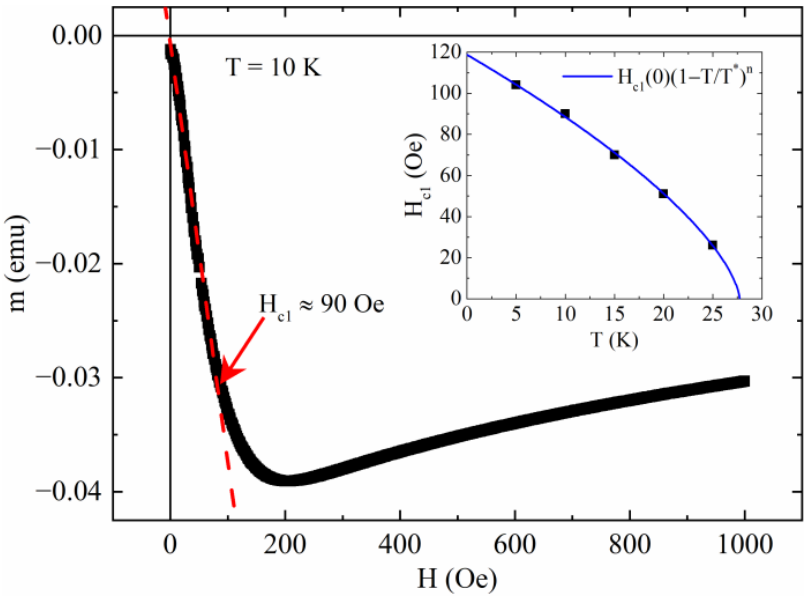

Figure 2. Field dependence of the magnetic moment curve for T = 10 K. The red dashed line corresponds to the linear behavior due to the Meissner state while the red arrow indicates the H_{c1} value. Inset: H_{c1} versus T data are fitted with $H_{c1} = H_{c1}(0)\ (1 - T/T^*)^n$. Fit results are reported in the text.

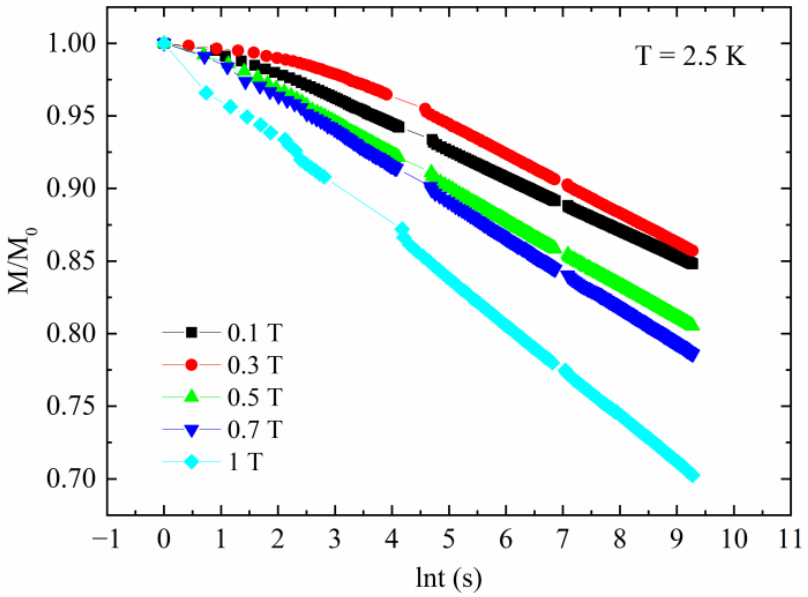

Figure 3. Time dependence of magnetization at different magnetic fields at T = 2.5 K.

From Figure 3, the pinning energy versus field U(H) values have been extracted by means of $U = -Tdln(t)/dln(|M|)$ [30,31]. In Figure 4, the U(H) for T = 2.5 K has been shown. It can be noted how the U(H) behavior changes for increasing fields. When the field is low, U(H) decrease is slow while the U(H) decrease is faster when the field is increased. These curve behaviors were fitted with $U(H) \propto H^{-\alpha}$ where α specifies the pinning regime of the sample.

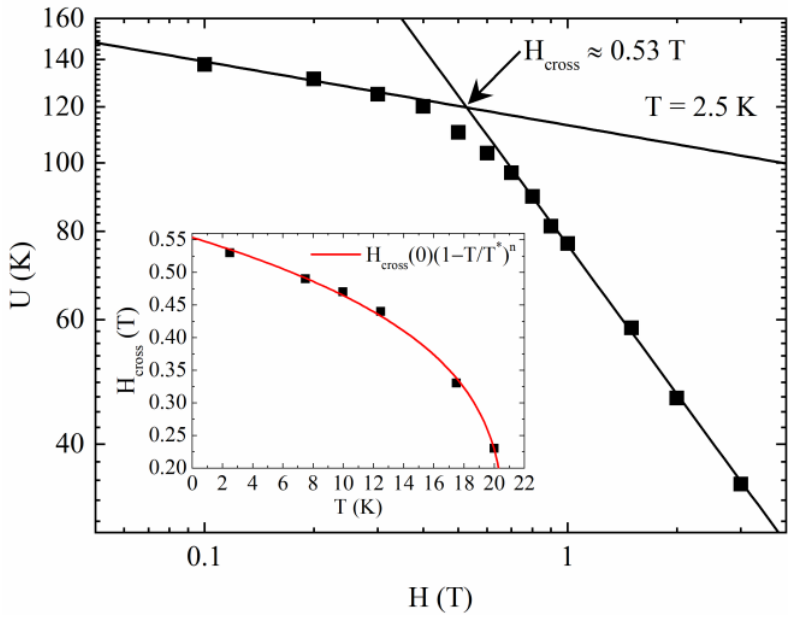

Figure 4. Field dependence of the pinning energy at 2.5 K. The data are fitted with the power law $U(H) \propto H^{-\alpha}$. Fit details are reported in the text. Inset: H_{cross} versus T data are fitted with $H_{cross} = H_{cross}(0)\ (1 - T/T^*)^n$. Fit results are reported in the text.

Specifically, a single vortex pinning regime is obtained when $\alpha \approx 0$ [32] while a collective pinning regime is individuated by $\alpha > 0.5$ [33]. From the fitting procedure, the field where the U(H) behavior changes was obtained, i.e., $H_{cross} \approx 0.53$ T. When $H < H_{cross}$, $\alpha \approx 0.09$ indicates that the vortices do not interact with each other (single vortex regime). When $H > H_{cross}$, $\alpha \approx 0.7$ indicates a collective pinning behavior. The same fitting procedure can be repeated at different temperatures. The temperature dependence of H_{cross} as is shown in the inset of Figure 4 together with its fit with the power law

$$H_{cross}(T) = H_{cross}(0)(1 - T/T^*)^n \quad (2)$$

where $H_{cross}(0) \approx 0.55$ T is the value of H_{cross} at T = 0 K, $T^* \approx 20.75$ K indicates when the phenomenon is undetectable, and $n \approx 0.27$ is the exponent. The study of $H_{cross}(T)$ line can be interesting since below it the sample shows a field behavior of the pinning energy almost constant which could allow a better transport of current. In order to find the irreversibility line, the critical current density J_c versus H curves have been shown in the main panel of Figure 5. A second magnetization peak phenomenon, similar to others observed in literature for iron-based superconductors [34–37], has been detected. The second peak position H_{sp}, individuated by a black dashed line in the main panel of Figure 5, typically identifies the transition between the elastic and the plastic distortion of the vortex lattice in the framework of a strong pinning [38–41]. The H_{sp} values have been extracted at the different temperatures and plotted in the inset(a) of Figure 5. In particular, the $H_{sp}(T)$ values have been fitted with the power law

$$H_{sp}(T) = H_{sp}(0)(1 - T/T^*)^n \quad (3)$$

where $H_{sp}(0) \approx 1.3$ T is the value of H_{sp} at T = 0 K, $T^* \approx 30.4$ K indicates when the phenomenon is undetectable, and $n \approx 0.14$ is the exponent. The $H_{sp}(T)$ line is very appealing for applications since for H approaching H_{sp} the J_c is increasing with the field while for $H > H_{sp}$ it is decreasing. On the other hand, the black solid line in the main panel of Figure 5 indicates the irreversibility field H_{irr} values. Specifically, H_{irr} can be obtained with

the criterion of J_c = 100 A/cm^2 [42]. In the inset(b) of Figure 5, H_{irr} versus temperature is shown together with the fit with the equation

$$H_{irr}(T) = H_{irr}(0)(1 - T/T^*)^n \quad (4)$$

where $H_{irr}(0) \approx 26$ T is the value of H_{irr} at T = 0 K, $T^* \approx 31.1$ K indicates when the phenomenon is undetectable, and $n \approx 0.86$ is the exponent. The $H_{irr}(T)$ line is very important since it individuates the vortex liquid region where no pinning forces act and high dissipations occur in the material. Naturally, this region must be avoided in the framework of power applications of superconductivity.

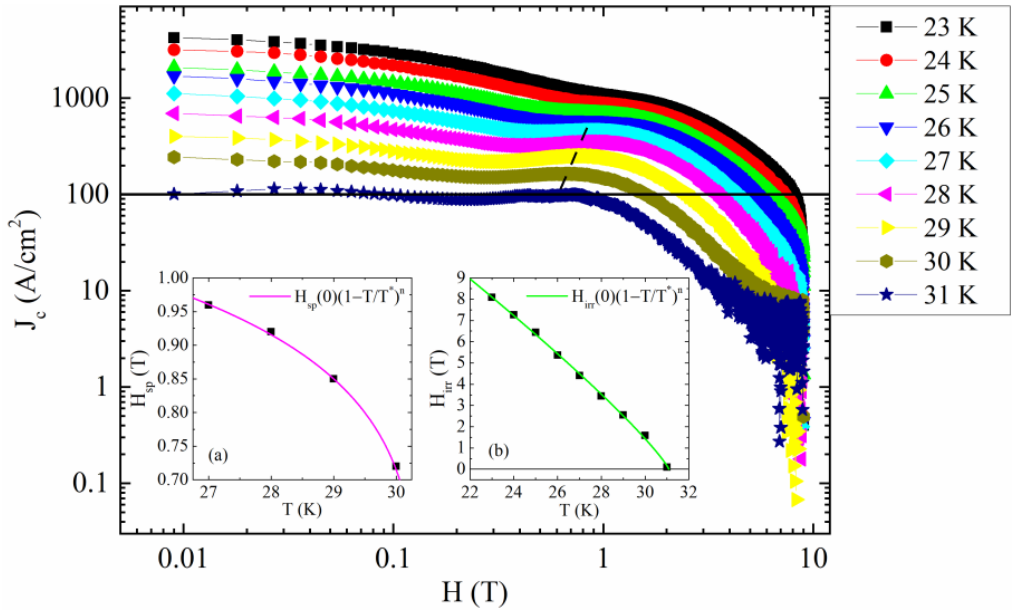

Figure 5. Critical current density J_c as a function of the field at different temperatures. The black horizontal line is the irreversibility line while the black dashed line individuates the second peak positions. Inset (**a**): Second peak values H_{sp} versus temperature. The data are fitted with the equation $H_{sp} = H_{sp}(0)\ (1 - T/T^*)^n$. Fit results are reported in the text. Inset (**b**): H_{irr} versus temperature. The data are fitted with the equation $H_{irr} = H_{irr}(0)\ (1 - T/T^*)^n$. Fit results are reported in the text.

Finally, m(T) curves have been performed in ZFC conditions at different magnetic fields (see the main panel of Figure 6) to evaluate the H_{c2} values. Particularly, they have been estimated by determining the onset of the magnetization drop at the different fields. $H_{c2}(T)$ curve is shown in the inset of Figure 6 together with the fit with the power law

$$H_{c2}(T) = H_{c2}(0)(1 - T/T_c)^n \quad (5)$$

where $H_{c2}(0) \approx 212$ T is the value of H_{c2} at T = 0 K, T_c = 35 K is the critical temperature of the sample at H ≈ 0 T [15], and $n \approx 0.9$ is the exponent. The $H_{c2}(T)$ line is important to determine the maximum appliable magnetic field to the material without its transition to the normal state.

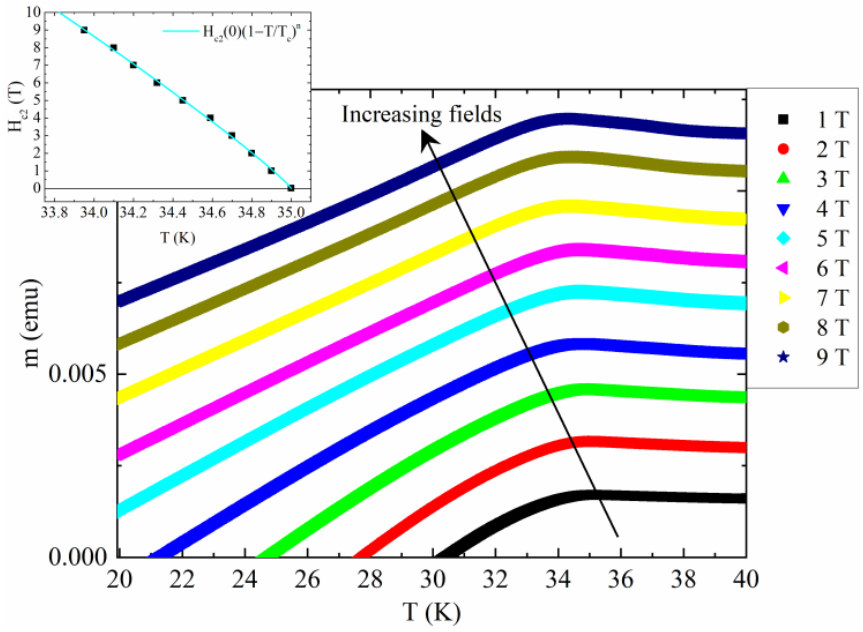

Figure 6. Magnetic moment as a function of the temperature in ZFC condition at different applied magnetic fields. Inset: H_{c2} versus T data are fitted with $H_{c2} = H_{c1}(0)\ (1 - T/T^{*})^{n}$. Fit results are reported in the text.

It is worth to underline the huge $H_{c2}(0)$ value which overcomes 200 T. Moreover, the n exponent values for H_{irr} and H_{c2} are minor than 1 different from what happens in iron-based materials of different families [36,43–47]. All the features discussed so far can be summarized by constructing the H(T) vortex phase diagram. In the main panel of Figure 7, H_{c1}, H_{irr}, H_{c2} are reported together with their fit. It is possible to note a very wide vortex liquid region where the vortices are unpinned [48–50]. In the framework of power applications of superconductivity, it is worth having the H_{irr} line near the H_{c2} one to hinder the vortices movement inside the material and the consequent dissipation with depression of critical current density. From this point of view, the sample must be optimized even if its critical current density values are in agreement with the literature [17,25,51]. It is worth to underline that the strong pinning region is very narrow compared with the vortex liquid one as shown in the main panel of Figure 7. This suggests the presence of a few strong pinning centers and a bad connection among the grains of the polycrystalline sample. This usually causes a fast J_c decrease as a function of the field due to the efficiency lack of the pinning acting in the sample which leads to wide vortex liquid regions. In the inset of Figure 7, the strong pinning region has been magnified. Even with the zoom, the region below the H_{c1} line is barely visible indicating a very weak Meissner state. Between the H_{c1} and H_{cross} lines, a single vortex behavior has been found. On the other hand, collective pinning characterized by elastic deformations of the vortex lattice can be noted between H_{cross} and H_{sp} lines. Between H_{sp} and H_{irr} lines, the plastic deformations rule the vortex dynamics of the sample. It is interesting to highlight that this plastic deformations area is the widest in the framework of the strong pinning region. When plastic deformations act in a sample, the pinning energy as a function of the temperature decreases quickly [52–54]. This is coherent with the weak pinning strength found in the sample. Finally, the next fascinating challenge is to improve the sample fabrication process in order to drastically reduce the vortex liquid region by nearing the H_{irr} line to the H_{c2} one. Reaching this target, a huge strong pinning region will be achieved allowing the sample to sustain high J_c in very high magnetic fields so becoming an interesting candidate for power applications of superconductivity.

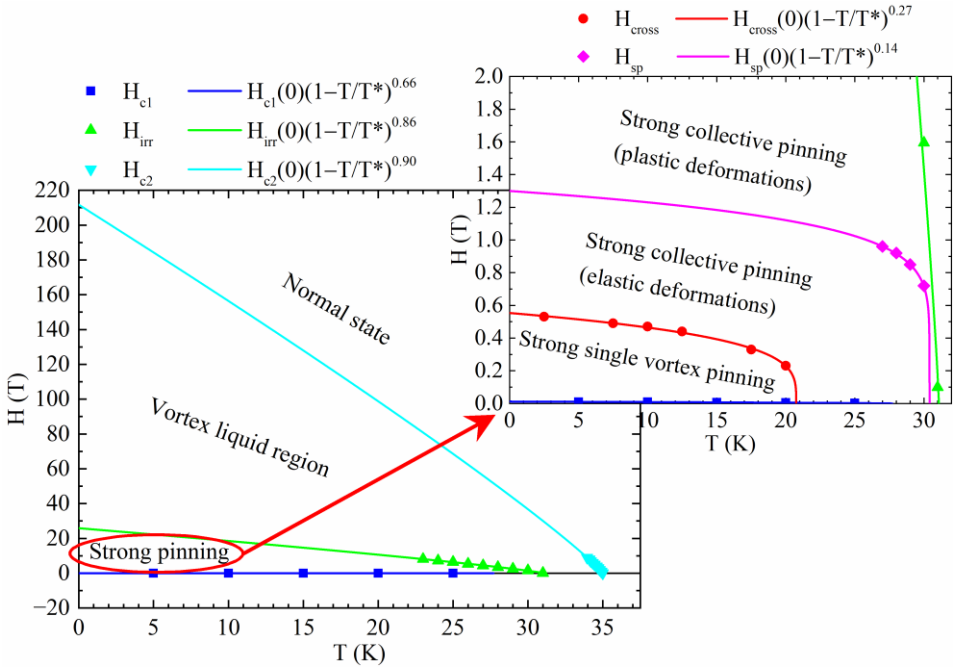

Figure 7. The H(T) vortex phase diagram of $CaKFe_4As_4$ polycrystalline sample. All the characteristic fields described in the main text are reported in the main panel and in the inset. The corresponding behaviors were fitted with the equation $H(T) = H(0)(1-T/T^*)^n$.

4. Conclusions

A $CaKFe_4As_4$ polycrystalline sample has been analyzed by means of DC magnetic measurements performed as a function of the temperature, the magnetic field, and the time in order to determine its superconducting critical parameters. By fitting all the reported characteristic fields with the power law $H(T) = H(0)(1 - T/T^*)^n$, a rich vortex phase diagram has been drawn showing a very wide vortex liquid region. An opening for the upcoming researchers can be to reduce this zero-pinning region by optimizing the fabrication process of the sample so making it more suitable for power applications. A further opening for future studies can also be the doping of non-optimized samples by using different elements in order to understand the behavior of the critical parameters analyzed in this work. Anyway, the study of non-optimized superconductors becomes very useful to understand how the superconducting critical parameters behave in presence of a magnetic field since this kind of sample can have an analogous magnetic behavior of wires and cables used in the power applications of superconductivity.

Author Contributions: Conceptualization, A.G., A.L., A.M. and F.V.; methodology, A.G. and A.L.; validation, A.G., A.L. and M.P.; formal analysis, A.G. and A.L.; investigation, A.G., A.L., A.M., A.N. and G.G.; data curation, A.G., A.L., A.M. and F.V.; writing—original draft preparation, A.G. and A.L.; writing—review and editing, A.M., F.V., A.N., G.G. and M.P.; visualization, A.N., G.G., M.P.; supervision, G.G. and M.P.; project administration, G.G. and M.P. All authors have read and agreed to the published version of the manuscript.

Funding: This research received no external funding.

Institutional Review Board Statement: Not applicable.

Informed Consent Statement: Not applicable.

Data Availability Statement: The data sets that support the findings in this study are available from the corresponding author upon reasonable request.

Conflicts of Interest: The authors declare no conflict of interest.

References

1. Kamihara, Y.; Watanabe, T.; Hirano, M.; Hosono, H. Iron-based layered superconductor La[O(1-x)F(x)]FeAs (x = 0.05-0.12) with T(c) = 26 K. *J. Am. Chem. Soc.* **2008**, *130*, 3296–3297. [CrossRef] [PubMed]
2. Bednorz, J.G.; Müller, K.A. Possible high Tc superconductivity in the Ba-La-Cu-O system. *Z. Phys. B Condens. Matter* **1986**, *64*, 189–193. [CrossRef]
3. Moodera, J.S.; Meservey, R.; Tkaczyk, J.E.; Hao, C.X.; Gibson, G.A.; Tedrow, P.M. Critical-magnetic-field anisotropy in single-crystal YBa2Cu3O7. *Phys. Rev. B* **1988**, *37*, 619–622. [CrossRef] [PubMed]
4. Naughton, M.J.; Yu, R.C.; Davies, P.K.; Fischer, J.E.; Chamberlin, R.V.; Wang, Z.Z.; Jing, T.W.; Ong, N.P.; Chaikin, P.M. Orientational anisotropy of the upper critical field in single-crystal $YBa_2Cu_3O_7$ and $Bi_{2.2}CaSr_{1.9}Cu_2O_{8+x}$. *Phys. Rev. B* **1988**, *38*, 9280–9283. [CrossRef] [PubMed]
5. Ambegaokar, V.; Baratoff, A. Tunneling Between Superconductors. *Phys. Rev. Lett.* **1963**, *10*, 486–489. [CrossRef]
6. Delin, K.A.; Kleinsasser, A.W. Stationary properties of high-critical-temperature proximity effect Josephson junctions. *Supercond. Sci. Technol.* **1996**, *9*, 227–269. [CrossRef]
7. Yuan, H.Q.; Singleton, J.; Balakirev, F.F.; Baily, S.A.; Chen, G.F.; Luo, J.L.; Wang, N.L. Nearly isotropic superconductivity in (Ba,K)Fe2As2. *Nature* **2009**, *457*, 565–568. [CrossRef]
8. Grimaldi, G.; Leo, A.; Martucciello, N.; Braccini, V.; Bellingeri, E.; Ferdeghini, C.; Galluzzi, A.; Polichetti, M.; Nigro, A.; Villegier, J.-C.; et al. Weak or Strong Anisotropy in Fe(Se,Te) Superconducting Thin Films Made of Layered Iron-Based Material? *IEEE Trans. Appl. Supercond.* **2019**, *29*, 1–4. [CrossRef]
9. Katase, T.; Ishimaru, Y.; Tsukamoto, A.; Hiramatsu, H.; Kamiya, T.; Tanabe, K.; Hosono, H. Advantageous grain boundaries in iron pnictide superconductors. *Nat. Commun.* **2011**, *2*, 409. [CrossRef]
10. De Gennes, P.G. Boundary effects in superconductors. *Rev. Mod. Phys.* **1964**, *36*, 225–237. [CrossRef]
11. Galluzzi, A.; Buchkov, K.; Nazarova, E.; Tomov, V.; Grimaldi, G.; Leo, A.; Pace, S.; Polichetti, M. Transport properties and high upper critical field of a Fe(Se,Te) iron based superconductor. *Eur. Phys. J. Spec. Top.* **2019**, *228*, 725–731. [CrossRef]
12. Fiamozzi Zignani, C.; De Marzi, G.; Corato, V.; Mancini, A.; Vannozzi, A.; Rufoloni, A.; Leo, A.; Guarino, A.; Galluzzi, A.; Nigro, A.; et al. Improvements of high-field pinning properties of polycrystalline Fe(Se,Te) material by heat treatments. *J. Mater. Sci.* **2019**, *54*, 5092–5100. [CrossRef]
13. Rotter, M.; Tegel, M.; Johrendt, D. Superconductivity at 38 K in the iron arsenide (Ba1-xKx)Fe2As2. *Phys. Rev. Lett.* **2008**, *101*, 107006. [CrossRef]
14. Iyo, A.; Kawashima, K.; Kinjo, T.; Nishio, T.; Ishida, S.; Fujihisa, H.; Gotoh, Y.; Kihou, K.; Eisaki, H.; Yoshida, Y. New-Structure-Type Fe-Based Superconductors: CaAFe4As4 (A = K, Rb, Cs) and SrAFe4As4 (A = Rb, Cs). *J. Am. Chem. Soc.* **2016**, *138*, 3410–3415. [CrossRef] [PubMed]
15. Galluzzi, A.; Leo, A.; Masi, A.; Varsano, F.; Nigro, A.; Grimaldi, G.; Polichetti, M. Critical Current and Pinning Features of a CaKFe4As4 Polycrystalline Sample. *Materials* **2021**, *14*, 6611. [CrossRef] [PubMed]
16. Meier, W.R.; Kong, T.; Kaluarachchi, U.S.; Taufour, V.; Jo, N.H.; Drachuck, G.; Böhmer, A.E.; Saunders, S.M.; Sapkota, A.; Kreyssig, A.; et al. Anisotropic thermodynamic and transport properties of single-crystalline CaKFe4As4. *Phys. Rev. B* **2016**, *94*, 064501. [CrossRef]
17. Singh, S.J.; Bristow, M.; Meier, W.R.; Taylor, P.; Blundell, S.J.; Canfield, P.C.; Coldea, A.I. Ultrahigh critical current densities, the vortex phase diagram, and the effect of granularity of the stoichiometric high-Tc superconductor CaKFe4As4. *Phys. Rev. Mater.* **2018**, *2*, 74802. [CrossRef]
18. Wang, C.; He, T.; Han, Q.; Ji, Z.; Lei, Q.; Tang, Q.; Li, Y.; Yu, B. Vortex creep activation energies and depinning currents in CaKFe4As4 and Ba0.6K0.4Fe2As2 revealed by AC susceptibility measurements. *J. Phys. Condens. Matter* **2020**, *32*, 415607. [CrossRef]
19. Cheng, Z.; Dong, C.; Huang, H.; Liu, S.; Zhu, Y.; Wang, D.; Vlasko-Vlasov, V.; Welp, U.; Kwok, W.K.; Ma, Y. Chemical stability and superconductivity in Ag-sheathed CaKFe4As4 superconducting tapes. *Supercond. Sci. Technol.* **2019**, *32*, 015008. [CrossRef]
20. Pyon, S.; Miyawaki, D.; Veshchunov, I.; Tamegai, T.; Takano, K.; Kajitani, H.; Koizumi, N.; Awaji, S. Fabrication and characterization of CaKFe4As4 round wires sintered at high pressure. *Appl. Phys. Express* **2018**, *11*, 123101. [CrossRef]
21. Adesso, M.G.; Polichetti, M.; Pace, S. Harmonics of the AC susceptibility for the study of I-V curves in melt grown YBCO. *Phys. C Supercond. Its Appl.* **2004**, *401*, 196–200. [CrossRef]
22. Senatore, C.; Polichetti, M.; Zola, D.; Matteo, T.D.; Giunchi, G.; Pace, S. Vortex dynamics and pinning properties analysis of MgB 2 bulk samples by ac susceptibility measurements. *Supercond. Sci. Technol.* **2003**, *16*, 183–187. [CrossRef]
23. Oliveira, A.A.M.; Hur, N.; Cheong, S.W.; Ortiz, W.A. Vortex glass melting in Mg-deficient MgB2. *Phys. Rev. B-Condens. Matter Mater. Phys.* **2010**, *82*, 104506. [CrossRef]
24. Oliveira, A.A.M.; Lisboa-Filho, P.N.; Ortiz, W.A. Solid-liquid transition in Nb powder determined by third harmonic susceptibility. *J. Magn. Magn. Mater.* **2008**, *320*, e510–e512. [CrossRef]
25. Masi, A.; Angrisani Armenio, A.; Celentano, G.; La Barbera, A.; Rufoloni, A.; Silva, E.; Vannozzi, A.; Varsano, F. Mechanochemically assisted low temperature synthesis route of the 1144 Ca-K Iron Based Superconductor. *Supercond. Sci. Technol.* **2020**, *33*, 74003–74010. [CrossRef]
26. Galluzzi, A.; Nigro, A.; Fittipaldi, R.; Guarino, A.; Pace, S.; Polichetti, M. DC magnetic characterization and pinning analysis on Nd1.85Ce0.15CuO4 cuprate superconductor. *J. Magn. Magn. Mater.* **2019**, *475*, 125–129. [CrossRef]

27. Polichetti, M.; Galluzzi, A.; Buchkov, K.; Tomov, V.; Nazarova, E.; Leo, A.; Grimaldi, G.; Pace, S. A precursor mechanism triggering the second magnetization peak phenomenon in superconducting materials. *Sci. Rep.* **2021**, *11*, 7247. [CrossRef]
28. Galluzzi, A.; Polichetti, M.; Buchkov, K.; Nazarova, E.; Mancusi, D.; Pace, S. Critical current and flux dynamics in Ag-doped FeSe superconductor. *Supercond. Sci. Technol.* **2017**, *30*, 025013. [CrossRef]
29. Felner, I.; Kopelevich, Y. Magnetization measurement of a possible high-temperature superconducting state in amorphous carbon doped with sulfur. *Phys. Rev. B-Condens. Matter Mater. Phys.* **2009**, *79*, 233409. [CrossRef]
30. Galluzzi, A.; Buchkov, K.M.; Nazarova, E.; Tomov, V.; Grimaldi, G.; Leo, A.; Pace, S.; Polichetti, M. Pinning energy and anisotropy properties of a Fe(Se,Te) iron based superconductor. *Nanotechnology* **2019**, *30*, 254001. [CrossRef]
31. Yeshurun, Y.; Malozemoff, A.P.; Shaulov, A. Magnetic relaxation in high-temperature superconductors. *Rev. Mod. Phys.* **1996**, *68*, 911–949. [CrossRef]
32. Blatter, G.; Feigel'Man, M.V.; Geshkenbein, V.B.; Larkin, A.I.; Vinokur, V.M. Vortices in high-temperature superconductors. *Rev. Mod. Phys.* **1994**, *66*, 1125–1388. [CrossRef]
33. Yeshurun, Y.; Malozemoff, A.P. Giant flux creep and irreversibility in an Y-Ba-Cu-O crystal: An alternative to the superconducting-glass model. *Phys. Rev. Lett.* **1988**, *60*, 2202–2205. [CrossRef]
34. Galluzzi, A.; Buchkov, K.; Tomov, V.; Nazarova, E.; Leo, A.; Grimaldi, G.; Nigro, A.; Pace, S.; Polichetti, M. Evidence of pinning crossover and the role of twin boundaries in the peak effect in FeSeTe iron based superconductor. *Supercond. Sci. Technol.* **2018**, *31*, 015014. [CrossRef]
35. Ionescu, A.M.; Miu, D.; Crisan, A.; Miu, L. Pinning-Induced Vortex-System Disordering at the Origin of the Second Magnetization Peak in Superconducting Single Crystals. *J. Supercond. Nov. Magn.* **2018**, *31*, 2329–2337. [CrossRef]
36. Pramanik, A.K.; Harnagea, L.; Nacke, C.; Wolter, A.U.B.; Wurmehl, S.; Kataev, V.; Büchner, B. Fishtail effect and vortex dynamics in LiFeAs single crystals. *Phys. Rev. B-Condens. Matter Mater. Phys.* **2011**, *83*, 094502. [CrossRef]
37. Miu, D.; Noji, T.; Adachi, T.; Koike, Y.; Miu, L. On the nature of the second magnetization peak in FeSe1−xTex single crystals. *Supercond. Sci. Technol.* **2012**, *25*, 115009. [CrossRef]
38. Yang, H.; Luo, H.; Wang, Z.; Wen, H.-H. Fishtail effect and the vortex phase diagram of single crystal Ba0.6K0.4Fe2As2. *Appl. Phys. Lett.* **2008**, *93*, 142506. [CrossRef]
39. Prozorov, R.; Ni, N.; Tanatar, M.A.; Kogan, V.G.; Gordon, R.T.; Martin, C.; Blomberg, E.C.; Prommapan, P.; Yan, J.Q.; Bud'ko, S.L.; et al. Vortex phase diagram of Ba(Fe0.93Co0.07)2As2 single crystals. *Phys. Rev. B* **2008**, *78*, 224506. [CrossRef]
40. Salem-Sugui, S.; Ghivelder, L.; Alvarenga, A.D.; Cohen, L.F.; Yates, K.A.; Morrison, K.; Pimentel, J.L.; Luo, H.; Wang, Z.; Wen, H.H. Flux dynamics associated with the second magnetization peak in the iron pnictide Ba1-xKxFe2As2. *Phys. Rev. B-Condens. Matter Mater. Phys.* **2010**, *82*, 054513. [CrossRef]
41. Sharma, S.; Vinod, K.; Sundar, C.S.; Bharathi, A. Critical current density and magnetic phase diagrams of BaFe 1.29Ru0.71As2 single crystals. *Supercond. Sci. Technol.* **2012**, *26*, 015009. [CrossRef]
42. Shabbir, B.; Wang, X.; Ghorbani, S.R.; Shekhar, C.; Dou, S.; Srivastava, O.N. Hydrostatic pressure: A very effective approach to significantly enhance critical current density in granular iron pnictide superconductors. *Sci. Rep.* **2015**, *5*, 8213. [CrossRef]
43. Shen, B.; Cheng, P.; Wang, Z.; Fang, L.; Ren, C.; Shan, L.; Wen, H.H. Flux dynamics and vortex phase diagram in Ba(Fe1-xCox)2As2 single crystals revealed by magnetization and its relaxation. *Phys. Rev. B* **2010**, *81*, 014503. [CrossRef]
44. Das, P.; Thakur, A.D.; Yadav, A.K.; Tomy, C.V.; Lees, M.R.; Balakrishnan, G.; Ramakrishnan, S.; Grover, A.K. Magnetization hysteresis and time decay measurements in FeSe 0.50Te 0.50: Evidence for fluctuation in mean free path induced pinning. *Phys. Rev. B-Condens. Matter Mater. Phys.* **2011**, *84*, 214526. [CrossRef]
45. Buchkov, K.; Galluzzi, A.; Mancusi, D.; Nazarova, E.; Pace, S.; Polichetti, M. Harmonic AC magnetic susceptibility analysis of FeSe crystals with composite morphology. *Phys. Scr.* **2019**, *94*, 085804. [CrossRef]
46. Galluzzi, A.; Buchkov, K.; Tomov, V.; Nazarova, E.; Leo, A.; Grimaldi, G.; Pace, S.; Polichetti, M. Mixed state properties analysis in AC magnetic field of strong pinning Fe(Se,Te) single crystal. *Supercond. Sci. Technol.* **2020**, *33*, 094006. [CrossRef]
47. Singh, S.J.; Shimoyama, J.; Yamamoto, A.; Ogino, H.; Kishio, K. Transition temperature and upper critical field in SmFeAsO 1-xFx synthesized at low heating temperatures. *IEEE Trans. Appl. Supercond.* **2013**, *23*, 7300605. [CrossRef]
48. Polichetti, M.; Adesso, M.G.; Pace, S. Response of glass and liquid phases in the vortex lattice to an external AC magnetic field at different frequencies. *Phys. A Stat. Mech. Its Appl.* **2004**, *339*, 119–124. [CrossRef]
49. Adesso, M.G.; Senatore, C.; Polichetti, M.; Pace, S. Harmonics of the AC susceptibility as probes to differentiate the various creep models. *Phys. C Supercond.* **2004**, *404*, 289–292. [CrossRef]
50. Marziali Bermúdez, M.; Pasquini, G.; Bud'Ko, S.L.; Canfield, P.C. Correlated vortex pinning in slightly orthorhombic twinned Ba(Fe1-xCox)2As2 single crystals: Possible shift of the vortex-glass/liquid transition. *Phys. Rev. B* **2013**, *87*, 054515. [CrossRef]
51. Singh, S.J.; Cassidy, S.J.; Bristow, M.; Blundell, S.J.; Clarke, S.J.; Coldea, A.I. Optimization of superconducting properties of the stoichiometric CaKFe4As4. *Supercond. Sci. Technol.* **2019**, *33*, 025003. [CrossRef]
52. Miu, L.; Miu, D. On the sensitivity of the Maley technique for the analysis of vortex-creep activation energy in disordered superconductors. *Supercond. Sci. Technol.* **2010**, *23*, 025033. [CrossRef]

53. Miu, L.; Miu, D.; Petrisor, T.; El Tahan, A.; Jakob, G.; Adrian, H. Origin of the plateau in the temperature dependence of the normalized magnetization relaxation rate in disordered high-temperature superconductors. *Phys. Rev. B-Condens. Matter Mater. Phys.* **2008**, *78*, 212508. [CrossRef]
54. El Tahan, A.; Jakob, G.; Miu, D.; Ivan, I.; Badica, P.; Miu, L. Vortex creep crossover in YBCO/PrBCO superlattices during standard magnetization relaxation measurements. *Supercond. Sci. Technol.* **2011**, *24*, 045014. [CrossRef]